

Alexandria Journal of Science and Technology



Article

Energy Gap of Some Binary and Ternary Semiconductor Alloys: Direct Calculations

K. Alfaramawi*, S. Abboudy, L. Abulnasr, Esraa M. Zahran

Department of Physics, Faculty of Science, Alexandria University, Alexandria 21511, Egypt.

* Correspondence Address:

K. Alfaramawi: Department of Physics, Faculty of Science, Alexandria University, Alexandria 21511, Egypt Email: kalfaramawi@alexu.edu.eg.

KEYWORDS: Energy gap, binary semiconductor alloy, ternary semiconductor alloy, Vegard's law, bowing parameter model.

Received:

August 30, 2025
Accepted:

September 22, 2025

Published:

October 27, 2025

ABSTRACT: The electrical and optical characteristics of semiconductor alloys, as well as their applicability for advanced device applications, are largely determined by the energy band gap. This study uses direct computational methods to examine the band gap of some chosen binary and ternary semiconductor alloys in the pure, doped non-degenerate, and doped degenerate regimes. Vegard's rule was utilized to estimate the compositional dependency of the band gap for binary alloys while a quadratic relation with bending parameters was used to describe ternary systems to capture non-linear behavior. Using a Lanyon–Tuft and semi-empirical approaches, carrier-induced band gap modulation in doped alloys was assessed, giving precise predictions for both degenerate and non-degenerate doping levels. The findings suggest that changes in alloy composition may cause the band gap to shift in a monotonic or non-linear manner. Moreover, higher doping typically leads to a band gap narrowing while the effect of temperature shows material-dependent patterns and frequently behave similarly to Varshni. Highperformance applications in optoelectronic, photonic, and high-frequency devices are made possible by these results, which provide crucial insights for the design and optimization of semiconductor alloys with customized electrical properties.

1. INTRODCTION

One crucial factor affecting the electrical and optical characteristics of semiconductor alloys is their energy gap (E_g) [1]. The energy gap of both binary and ternary semiconductor alloys is greatly influenced by many factors such as crystal structure, alloy composition, temperature and doping level [2-3]. As an example, for Ga_xAs_{1-x} binary alloy, the energy gap is altered by variation of the composition parameter (x) and it changes as temperature rises due to lattice expansion, which decreases the overlap between the valence and conduction bands [3]. Nevertheless, the variation of binary alloy energy gap may result from the addition of various elements to the crystal lattice. For example, the optical and electronic behaviour of GaAs can be altered by the introduction of localized electronic states close to the band boundaries when impurity is added [4-5].

For ternary systems, by changing the composition parameter, ternary semiconductor alloys provide energy gap tunability [6]. Even so, there is sometimes a phenomenon called "band gap bowing" in the relationship between composition and energy gap, which is not necessarily linear. A deviation from the linear interpolation between the energy gaps of the constituent binary compounds is caused by this bending effect [7]. Variations in

atomic size mismatch, electronegativity difference and strain effects are some of the factors that affect the degree of bowing in ternary alloys. Various empirical models have been put up to explain this dependence [8-11].

In the last decades, many works have been done to achieve the parameters affecting the energy gap in binary and ternary semiconductor alloys. As examples, Khomyakov et al. [12] used first-principles simulations to study the compositional dependency of band energies in strained $In_xGa_{1-x}As$ ternary alloys. They discovered that the overall band gap is impacted by the conduction and valence band boundaries with notable nonlinear bowing as the indium content rises. According to the results, strain further alters the band gap and deformation potentials, offering crucial quantitative information for device design. Among the drawbacks are the neglect of temperature and defective effects, which could affect practical applications [12,14].

Shen et al. [13] examined band bending and the direct-to-indirect band gap crossover in random $B_x A l_{1-x} N$ alloys using first-principles calculations. They showed how the band gap changes from a direct to an indirect gap at greater B concentrations due to a nonlinear reduction with rising boron

content. Their research offers crucial quantitative instructions for adjusting the electrical characteristics of $B_xAl_{1-x}N$ alloys for optoelectronic uses [13,15]. The inverse relationship between temperature and band gap is confirmed in a variety of systems such as $Ge^{1-}_xSi_x$, $Ge_{1-x}Sn_x$ and $ZnSe_{1-x}O_x$ [16-18].

Previous studies examining how temperature affects the energy band gap in semiconductors have examined a variety of materials, such as $CuSiP_3$ and $Al_xGa_{1-x}N$, and have consistently shown that the band gap reduces as temperature rises [19-20]. Using the PSOPW approach, Abdullah et al. theoretically studied $CuSiP_3$ and demonstrated that phononinduced vibrations outweigh lattice expansion, resulting in a decrease in the band gap with increasing temperature [19]. Using deep-ultraviolet photoluminescence spectroscopy, Nepal et al. experimentally investigated $Al_xGa_{1-x}N$ alloys throughout a temperature range of 10–800 K. They found that the Varshni coefficients increased in proportion to composition and that the band gap decreased nonlinearly with temperature [20].

Even though binary and ternary semiconductor alloys have been the subject of substantial research, most studies have focused on the effects of temperature, composition, or doping separately, usually in small-scale systems or simplified theoretical models. There are several reports on electrical and optical characteristics, such as the energy band gap, but there are still a few systematic quantitative investigations that simultaneously analyze the combined effects of temperature, concentration, and composition. The present work intends to create a thorough computational framework for analyzing and forecasting the energy gap of certain III-V and II-VI semiconductor alloys under a range of physical circumstances. There are three main goals for this work: (1) using Vegard's law and bowing parameter models, quantifying the impact of alloy composition on the band structure; (2) using the Lanyon-Tuft and semi-empirical approaches, investigating the role of doping in both non-degenerate and degenerate regimes; (3) evaluating the temperature dependence of these properties across all regimes. Predictive methods for optimizing performance in optoelectronic and microelectronic systems working under various functional and environmental situations are provided by the findings, which provide important insights into the interdependent behavior of structural and electronic variables.

2. Theoretical Model

2.1. Energy gap of binary semiconductor alloys

The energy gap of binary semiconductor alloy A_{1-x} B_x can be calculated by Vegard's law [21]:

$$E_g^{alloy}(x) = E_g^{AB}(x) = xE_g^B + (1-x)E_g^A$$
 (1)

where E_g^A and E_g^B are the energy gaps of the elements A and B and x is the composition of the element B.

2.1.1. Undoped Binary Alloys

In the case of *undoped binary* semiconductor alloy, both E_g^A and E_g^B will be substituted by their known undoped values for each element A and B respectively. The energy gap of the binary alloy is calculated from Vegard's law (equation 1), which is used directly to study the dependence of the alloy energy gap on the composition of the alloy.

2.1.2. Doped Non-Degenerate Binary Alloys

In the case when the binary semiconductor alloys are doped with impurities of a concentration (N_d) less than the effective density of states in the conduction band of the alloy (N_c) , the alloys will be non-degenerate, thus E_g^A and E_g^B will be calculated by non-degenerate Lanyon and Tuft approach [22-23]:

$$E_g(T,N) = E_{g,0} - \frac{3e^2}{16\pi\varepsilon} \left(\frac{e^2N}{\varepsilon k_B T}\right)^{\frac{1}{2}}$$
 (2)

where N is the total carrier concentration (m^{-3}) , $E_{g,0}$ is the energy gap at 0 K, T is the absolute temperature, e is the electronic charge, K_B is Boltzmann's constant and ε is the dielectric permittivity of the host material. Equation 2, with the aid of equation 1, is used to investigate the effect of both temperature and doping concentration on the binary alloy.

2.1.3. Doped Degenerate Binary Alloys

When the binary semiconductor alloys are doped with a concentration (N_d) greater than the effective density of states in the conduction band of the alloy (N_c) , the alloy will be degenerate and E_g^A , E_g^B , E_g^{AB} will be calculated by degenerate Lanyon and Tuft approach and the semi-empirical approach.

The Lanyon and Tuft's approach for degenerate case is given by [22-23]:

$$E_g(N) = E_{g,0} - \frac{3e^2}{16\pi\varepsilon} \left(\frac{8}{3\sqrt{\pi}}\right)^{\frac{1}{3}} \left(\frac{3\pi e^2 m^*}{\varepsilon h^2}\right)^{\frac{1}{2}} N^{\frac{1}{6}}$$
 (3)

where m^* is the electron effective mass and h is Planck's constant.

The equation of semi-empirical approach for degenerate case describes the energy gap as a function of both donors and temperature which is given by [24-25]:

$$E_g(T, N) = E_{g,0} - \frac{\alpha T^2}{\beta + T} - 2N^{\frac{1}{3}}$$
 (4)

where α & β are the material-specific constants related to the temperature dependence of the band gap.

2.2. Energy Gap of Ternary Semiconductor Alloys

The energy gap of ternary alloy AB_xC_{1-x} is described by bowing parameter model [26]:

$$E_g^{alloy}(x) = E_g^{ABC}(x) = xE_g^{AB} + (1-x)E_g^{AC} - C^{ABC}x(1-x)$$
 (5)

where E_g^{AB} and E_g^{AC} are the energy gaps of compounds AB and AC, respectively, C^{ABC} is the bowing parameter and x is the composition of the compound AB.

2.2.1. Undoped Ternary Semiconductor Alloys

In the case of undoped ternary semiconductor alloy, the average energy gap of the compounds AB and AC (E_g^{AB} and E_g^{AC}) will be calculated by Phillips ionicity model [27-28]:

$$E_a^2 = E_h^2 + E_c^2 (6)$$

Where E_h is the homopolar energy gap (eV) and E_c is the heteropolar energy gap (eV) given by

$$E_h = 26.738. \ r_s^{-2.48} \tag{7}$$

$$E_c = 24.55b \left[\frac{Z_A^* - Z_B^*}{r_s} \right] e^{-1.7323r_s^{1/2}}$$
 (8)

where r_s is the electron density parameter and Z_A^* , Z_B^* are the valency of the compound's element components. It is easily demonstrated that $Z_A^* - Z_B^* = 4$ and 2, respectively for II-VI and III-V group semiconductors respectively, and thus we have

$$E_c(group III-V) = 49.10 \frac{b}{r_s} e^{-1.7323 r_s^{1/2}} (eV)$$

$$E_c(group II-VI) = 98.21 \frac{b}{r_s} e^{-1.7323 r_s^{1/2}} (eV)$$
(10)

$$E_c(group II-VI) = 98.21 \frac{b}{r_s} e^{-1.7323} r_s^{1/2} (eV)$$
 (10)

Consequently, after estimation of both E_q^{AB} and E_q^{AC} , one can use equation 5 to study the energy gap of the ternary alloy as a function of the composition in the non-doping state.

2.2.2. Doped Non-Degenerate Ternary Semiconductor **Alloys**

For doped non-degenerate ternary alloys, the energy gap of the compounds E_g^{AB} and E_g^{AC} will be calculated by non-degenerate Lanyon and Tuft approach, equation 2. After that, the values can be substituted in equation 5 to evaluate the energy gap of the ternary alloy. With this procedure, one can investigate the variation of the energy gap of the ternary alloy with the temperature and impurity doping concentration in the nondegeneracy state.

2.2.3. Doped degenerate ternary semiconductor alloys

In the case of doped degenerate ternary semiconductor alloys, the energy gap of the compounds E_q^{AB} and E_q^{AC} will be calculated by degenerate Lanyon and Tuft approach, equation 3 and semiempirical approach, equation 4. Consequently, the values can be substituted in equation 5 to evaluate the energy gap of the ternary alloy. With this procedure, one can depict the dependence of the energy gap of the doped degenerate ternary alloy on the temperature and impurity doping concentration.

3. Results and Discussion

3.1. Energy Gap of Binary Semiconductor Alloys

3.1.1. Undoped binary alloys

Figure 1 shows how the energy gap of undoped IV-IV binary semiconductor alloys at 300K varies with their composition (x). The energy gap E_g^{alloy} was calculated by Vegard's law (equation 1), whereas E_q^B , E_q^A were substituted by their known values for each element as shown in Table 1. It is clear from Figure 1 that E_a of the alloy increases with rising (x) in $Ge_{1-x} C_x$ and $Si_{1-x} C_x$. In contrast, E_q decreases with rising (x) in Si_{1-x} Ge_x . These results obtained a good agreement with previous work [29-30].

3.1.2. Doped Non-Degenerate Binary Alloys

Figure 2 demonstrates the effect of each of composition, temperature and doping concentration on the energy gap of the doped non-degenerate binary alloys. Figure 2a shows the energy gap versus composition of doped non-degenerate IV-IV binary semiconductor alloys. The computations are carried out at T = 300 K, $N_d = 8 \times 10^{17} \text{m}^{-3}$ and $N = 1.75 \times 10^{23} \text{m}^{-3}$. The alloy energy gap $E_g^{alloy}(x)$ is calculated by Vegard's law, whereas both E_g^B and E_g^A are determined based on nondegenerate Lanyon and Tuft approach (equation 2) utilizing the constants provided in Table 1. One can notice from Figure 2a

that E_q increases with rising the alloy composition in $Ge_{1-x} C_x$ and $Si_{1-x} C_x$. In contrast, E_q decreases with rising (x) in $Si_{1-x} Ge_x$. The results agree well with the data previously obtained [29-30].

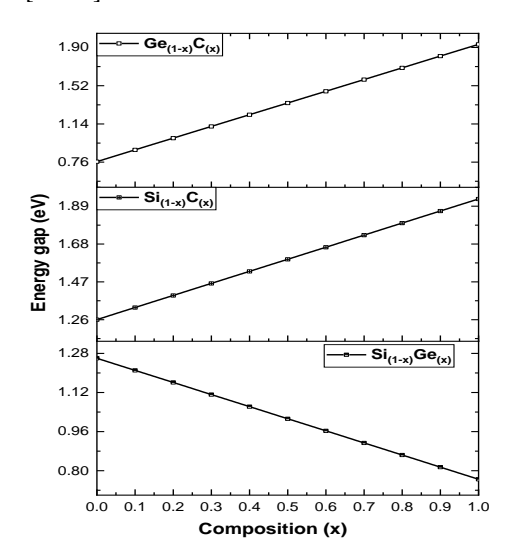


Figure 1. Energy gap of some selected undoped IV-IV binary semiconductor alloys versus composition at 300 K.

Figure 2b shows the effect of temperature on the energy gap of non-degenerately doped $Si_{0.5}$ $Ge_{0.5}$ where doping concentrations are fixed at $N_d=4.5\times 10^{19}~m^{-3}$, 6 $\times 10^{19}~m^{-3}$, and 7.5 $\times 10^{19}~m^{-3}$ in a temperature range up to 450 K. The alloy energy gap $E_g^{alloy}(x)$ was calculated by Vegard's law, whereas both E_a^B and E_a^A are determined from the non-degenerate Lanyon and Tuft approach (equation 2) using the constants in Table 1. Figure 2b demonstrates that the energy gap increased with increasing temperature until about 100-150 K.

Above this range, the rate of increase is very slow, with the energy gap indicating a trend towards saturation at higher temperatures. Furthermore, increasing doping concentration at any selected temperature resulted in a little decrease in the energy gap [31-32].

Figure 2c shows the relation between the energy gap and donor concentrations of doped non-degenerate $Si_{0.5}Ge_{0.5}$ at some selected temperatures 200 K, 300 K and 400 K. Again $E_g^{alloy}\left(x\right)$ used Vegard's law equation 1, whereas both E_g^B and E_a^A are determined based on non-degenerate Lanyon and Tuft equation 2. The calculations are processed at total carrier concentration of $N = 1.75 \times 10^{23} \text{ m}^{-3}$ and the constants provided in Table 1. It is depicted from the figure that the energy gap decreases slightly with increasing donor concentration. At greater donor concentrations, the change in energy gap becomes more significant. Higher temperatures usually result in slightly energy gap values for a given donor concentration. The results are in a good agreement with the data that was previously published [33-34].

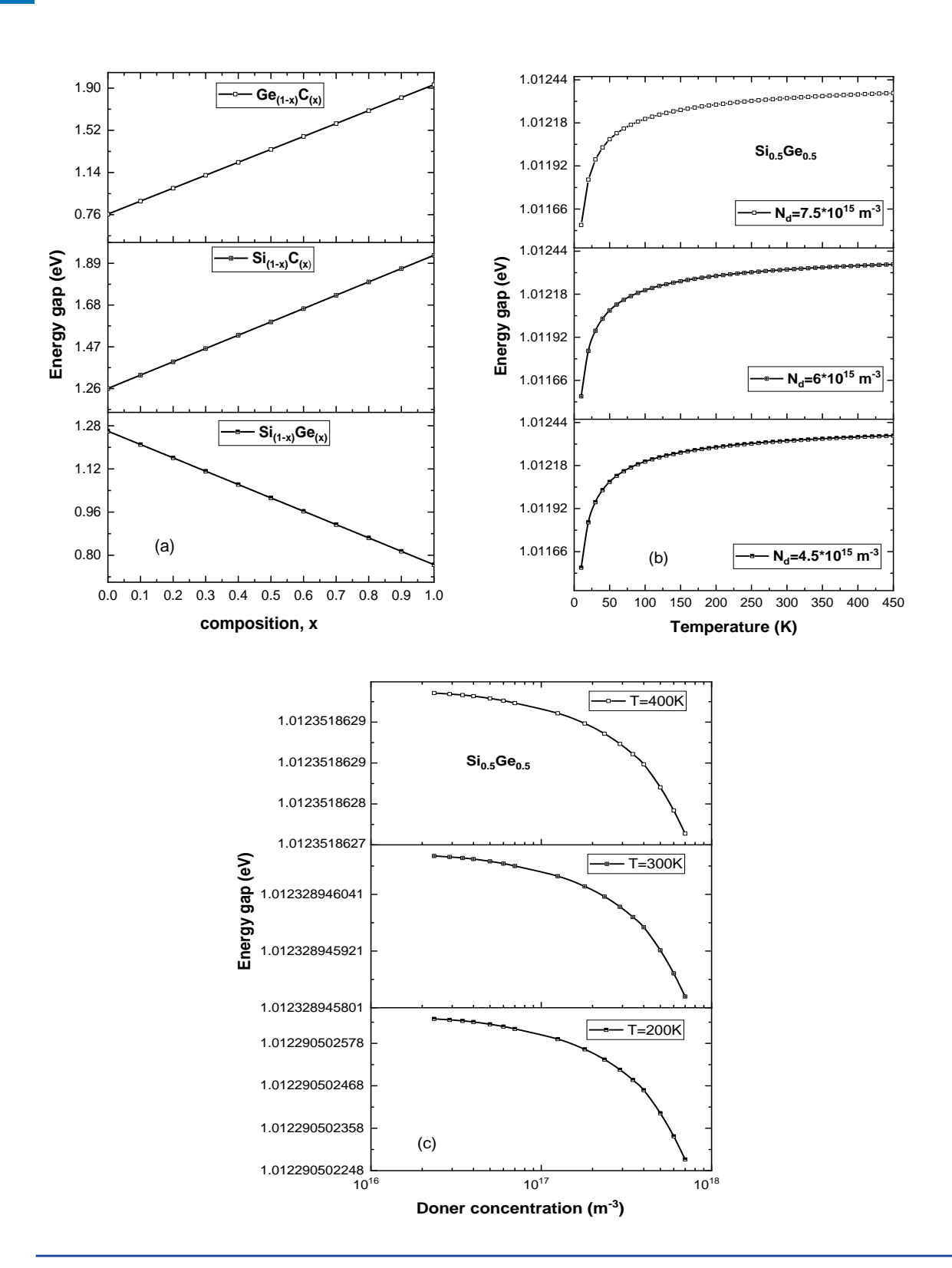


Figure 2. Energy gap of doped non-degenerate IV-IV binary semiconductor alloys according to Lanyon and Tuft approach versus (a) alloy composition at 300K. (b) temperature, (c) donor concentration.

3.1.3. Doped Degenerate Binary Alloys

For doped degenerate binary semiconductor alloys, the effect of composition, temperature and doping concentration on the energy gap of such systems is investigated. Figure 3a shows the energy gap versus composition for some selected IV-IV binary semiconductor alloys at 300 K and $N_d = 3 \times 10^{18} \text{m}^{-3}$. The binary alloy band gap $E_g^{alloy}(x)$ is calculated by Vegard's law, whereas the band gaps of the constituent elements E_q^B and E_q^A are determined based on degenerate Lanyon and Tuft approach (equation 3). The total number of carriers are set to be $N = 1.70 \times 10^{23} \ m^{-3}$ utilizing the constants provided in Table 1. One can notice from Figure 3a that the energy gaps of both $Ge_{1-x} C_x$ and $Si_{1-x} C_x$ alloys increase continuously as the carbon composition (x) increases whereas the energy gap for Si_{1-r} Ge_r decreases continuously as the composition of Germanium increases. These results are fairly match with the data reported in references [35-36].

Figure 3b shows the energy gap of $Si_{0.5}Ge_{0.5}$ at various donor concentrations $3.5 \times 10^{18} m^{-3}$, $1.3 \times 10^{19} m^{-3}$, and $1.03 \times 10^{20} m^{-3}$ as a function of temperature calculated using the semi-empirical approach (equation 4). The same procedure was followed to calculate $E_g^{alloy}(x)$, E_g^B and E_g^A . The total number of carriers was taken as $N = 1.70 \times 10^{23} m^{-3}$, and the constants used in the calculations as provided in Table 1. The energy gap decreases with rising temperature across all examined doping concentrations; this may be attributed because thermal excitation causes lattice vibrations that narrow the band gap. Thus, the inverse relationship between temperature and band gap is confirmed by this behavior, which has been observed in a variety of systems [16-17]. Also, it is obvious from **Figure 3b** that at fixed temperature, increasing the doping concentration appears to result in a little decrease in the energy gap value. The results obtained show good agreement with the data that was previously presented [37-38].

Figure 3c shows the relationship between the energy gap of doped degenerate $Si_{0.5}Ge_{0.5}$ and donor concentrations at nominated temperatures 200 K, 300 K, and 400 K calculated according to Lanyon and Tuft's approach (equation 3) at $N=1.75\times 10^{23}~m^{-3}$, and the constants provided in Table 1. The energy gap decreases slightly with increasing donor concentration. At greater donor concentrations, the change in energy gap becomes more significant. Higher temperatures usually result in slightly lower energy gap values for a given donor concentration [39-40].

3.2. Energy Gap of Ternary Semiconductor Alloys

3.2.1. Undoped Ternary Alloys

Figure 4 depicts the energy gap versus alloy composition of some undoped III-V and II-VI ternary semiconductor alloys. **Figure 4a** shows the energy gap of some selected undoped III-V ternary semiconductor alloys versus composition at 300 K. The alloy energy gap $E_g^{alloy}(x)$ is calculated by bowing parameter model (equation 5), whereas both E_g^{AB} and E_g^{AC} of the compounds AB and AC are determined based on Phillips ionicity model (equation 6), E_h and E_c are determined by equations 7 and 9 respectively.

The parameters used in the calculations are listed in Table 2.

Figure 4a obtains that the energy gap of both $AlAs_{(x)}Sb_{(1-x)}$ and $GaP_{(x)}As_{(1-x)}$ decreases continuously as the compositions of AlAs and GaP increase, respectively, while for $GaSb_{(x)}P_{(1-x)}$, the energy gap is, initially, decreasing with increasing of GaSb composition up to about x = 0.4 and then increasing with further elevation of x. On the contrary, the energy gap of $GaAs_{(x)}Sb_{(1-x)}$ increases as the GaAs composition increases [37–40].

Figure 4b shows the energy gap of nominated undoped II-VI ternary semiconductor alloys versus composition at 300K. The energy gap $E_g^{alloy}(x)$ is calculated by bowing parameter model, equation (5), whereas both E_g^{AB} and E_g^{AC} are determined based on Phillips ionicity model, equation (6), E_h and E_c are determined by equations (7) and (10), respectively. Table 2 shows the parameters used in this calculation. For the alloys $CdS_{(x)}Se_{(1-x)}$, $CdSe_{(x)}Te_{(1-x)}$ and $ZnSe_{(x)}S_{(1-x)}$, the behaviour of energy gap is, initially, almost constant up to about x = 0.25, and after this value, it increases with rising of the composition. On the other hand, the energy gap of $ZnTe_{(x)}Se_{(1-x)}$ decreases as the ZnTe composition increases [35-36,41-42].

3.2.2. Doped Non-Degenerate Ternary Alloys

The dependence of the energy gap of some selected doped nondegenerate III-V and II-VI semiconductor ternary alloys on the alloy composition is depicted in **Figure 5**, but the dependence on the temperature is shown in **Figure 6** whereas **Figure 7** shows the variations with the donor concentrations.

Figure 5a shows the energy gap of doped non-degenerate III-V ternary semiconductor alloys versus composition at 300K and $N_d = 9 \times 10^{17} \text{m}^{-3}$. The alloy energy gap is calculated by bowing parameter model, whereas both E_q^{AB} and E_q^{AC} are determined based on non-degenerate Lanyon and Tuft approach and the constants from Table 2. It is obvious from Figure 5a energy gaps of $AlAs_{(x)}Sb_{(1-x)}$ and $GaP_{(x)}As_{(1-x)}$ decrease continuously by elevation of AlAs and GaP compositions respectively. Alternatively, the energy gap for $GaSb_{(x)}P_{(1-x)}$ is non-linear, initially decreasing with increasing GaSb composition up to around x=0.4 and then increasing. The energy gap of $GaAs_{(x)}Sb_{(1-x)}$ increases as the GaAs composition increases.

Comparing the results of energy gap of undoped and doped III-V ternary semiconductor alloys with alloy compositions (**Figures 4a & 5a**), leads one to observe the similarity in the energy gap behviour [37–40].

Figure 5b shows the energy gap of doped non-degenerate II-VI ternary semiconductor alloys versus composition at 300K and $N_d = 1 \times 10^{18} \text{m}^{-3}$ determined based on bowing parameter approach and non-degenerate Lanyon and Tuft equation. **Figure 5b** demonstrates that the energy gap trends of doped II-VI ternary semiconductor alloys with alloy compositions are similar to those of undoped alloys (**Figure 4b**) [35-36,41-42].

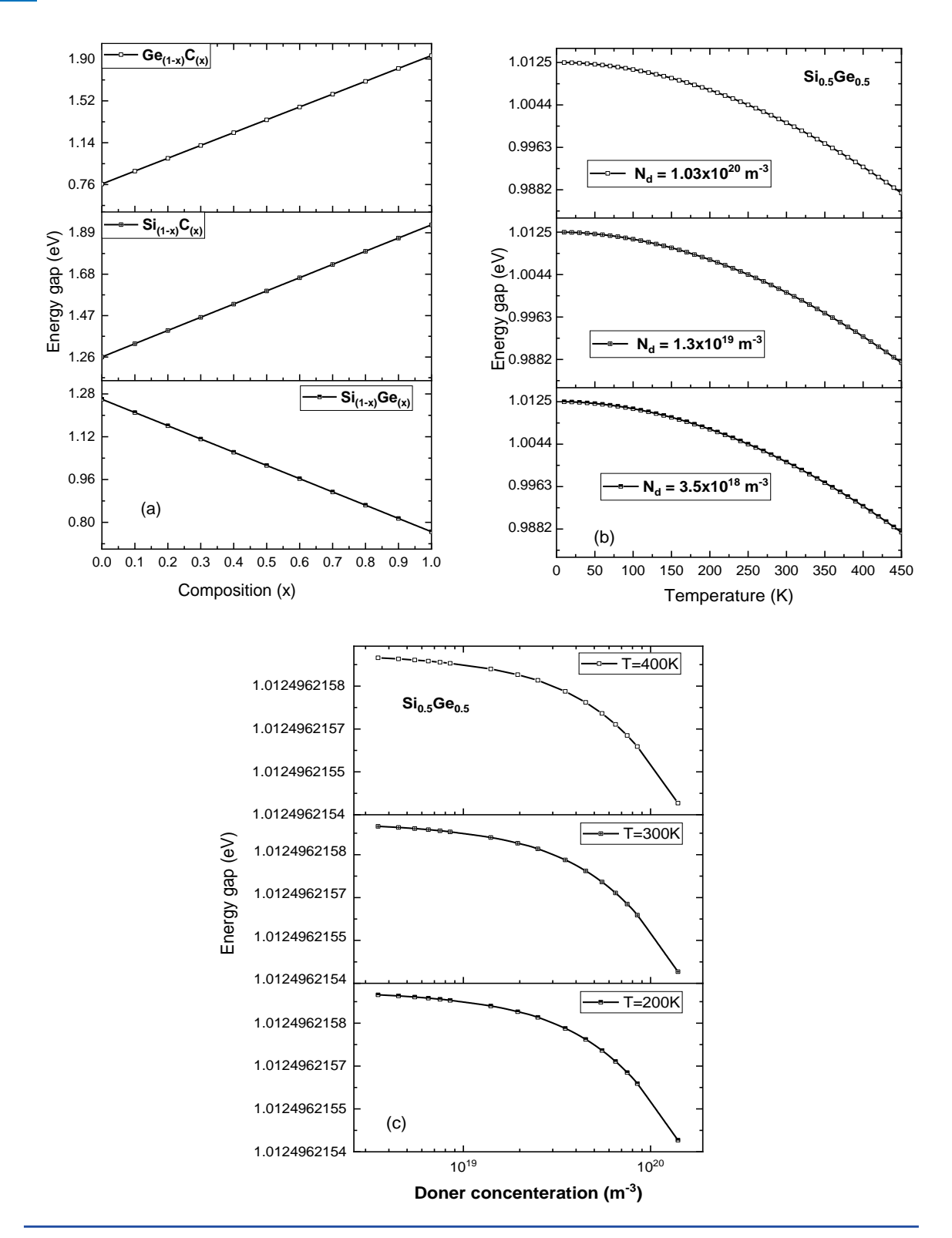


Figure 3. The energy gap of (a) some selected IV-IV semiconductor alloys versus composition at 300K calculated according to Lanyon and Tuft's approach (equation 3), (b) $Si_{0.5}Ge_{0.5}$ alloy versus temperature calculated from the semi-empirical approach (equation 4), (c) $Si_{0.5}Ge_{0.5}$ alloy versus doner concentration due to Lanyon and Tuft's approach (equation 3).

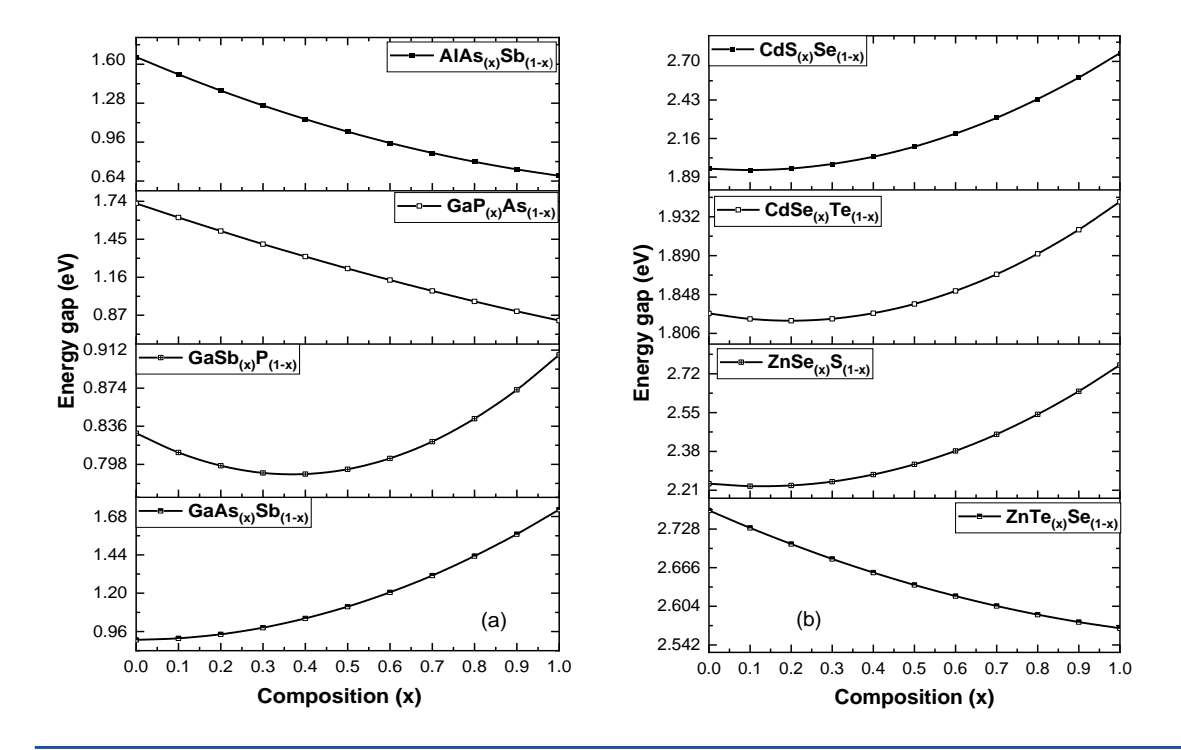


Figure 4. Energy gap versus composition at 300 K of (a) undoped III-V ternary semiconductor alloys, (b) undoped II-VI ternary semiconductor.

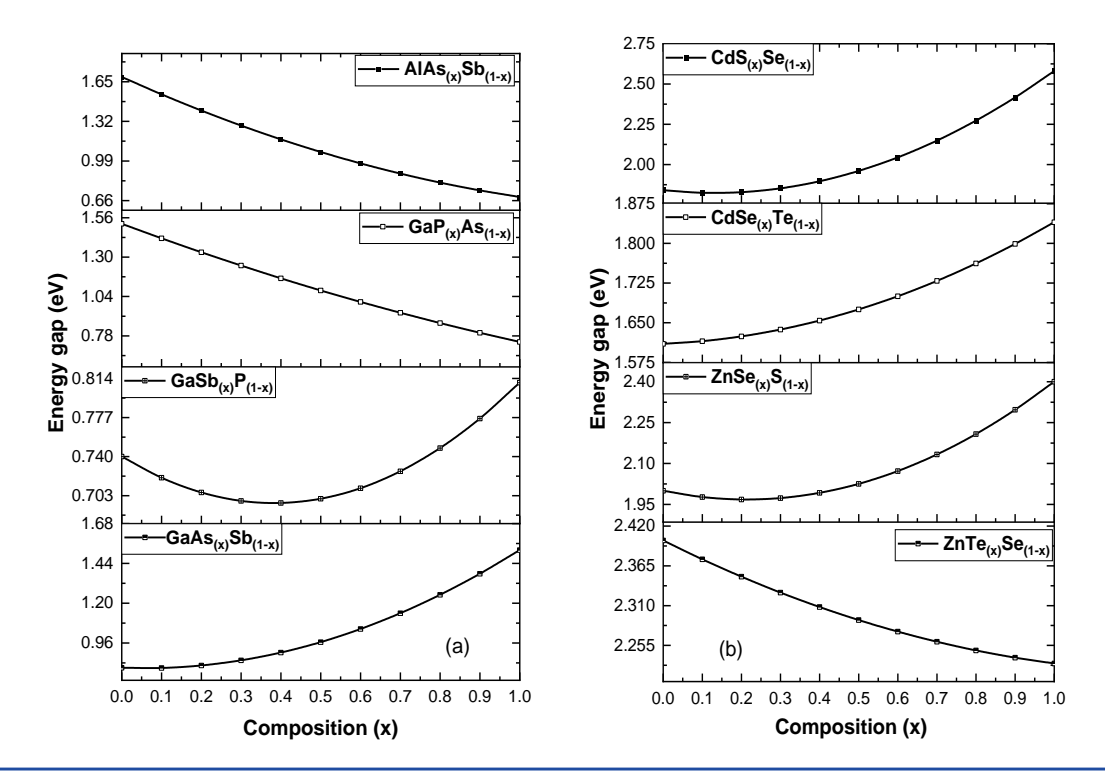


Figure 5. Energy gap versus composition at 300K according to Lanyon and Tuft approach of (a) doped non-degenerate III-V ternary semiconductor alloys, (b) doped non-degenerate II-VI ternary semiconductor alloys.

Figures 6a & 6b show the effect of temperatures up to 450 K on the energy gap of non-degenerately doped $GaAs_{0.5}Sb_{0.5}$ (as example of III-V ternary alloys) and $CdSe_{0.5}Te_{0.5}$ (as example of III-VI ternary alloys), respectively, at three various doping concentrations according to doped non-degenerate Lanyon and Tuft approach and bowing parameter model and the constants provided in Table 2. The trend of the energy gaps with temperature are similar for the two alloys. The energy gap rises fast with increasing temperature, until about 100-150 K. Above this range, the rate of increase becomes very slow expecting a saturation trend at higher temperatures. Furthermore, increasing doping concentration throughout the examined temperature range resulted in a little decrease in the energy gap [43-44].

Figures 7a and 7b illustrate the relationship between the energy gap and donor concentrations of doped non-degenerate $GaAs_{0.5}Sb_{0.5}$ (III-V ternary alloy) and $CdSe_{0.5}Te_{0.5}$ (II-VI ternary alloy) at some selected temperatures (200 K, 300 K, and 400 K). The calculations utilize doped non-degenerate Lanyon and Tuft approach and bowing parameter model and the constants provided in Table 2. It is noticeable from the Figures that the energy gap decreases slightly with increasing donor concentrations. At greater donor concentrations, the change in

energy gap becomes more significant. Higher temperatures usually result in slightly lower energy gap values for a given donor concentration [37-40].

3.2.3. Ternary doped degenerate semiconductor alloys

Variation of the energy gap with the alloy composition, temperature and doping concentration is depicted in **Figures 8, 9 & 10** for selected doped degenerate III-V and II-VI semiconductor ternary alloys. **Figure 8a** shows the energy gap of some doped degenerate III-V ternary semiconductor alloys versus composition at 300K and $N_d = 2 \times 10^{19} \mathrm{m}^{-3}$. The calculation uses bowing parameter model, doped degenerate Lanyon and Tuft approach and the constants in **Table 2**. The energy gap of $AlAs_{(x)}Sb_{(1-x)}$ and $GaP_{(x)}As_{(1-x)}$ alloys decrease continuously as the AlAs and GaP fractions increase, respectively. Contrary, the energy gap of $GaSb_{(x)}P_{(1-x)}$ is initially decreasing with increasing GaSb composition up to around x = 0.4 and then increasing, whereas the energy gap of $GaAs_{(x)}Sb_{(1-x)}$ increases as the GaAs composition increases [37-40].

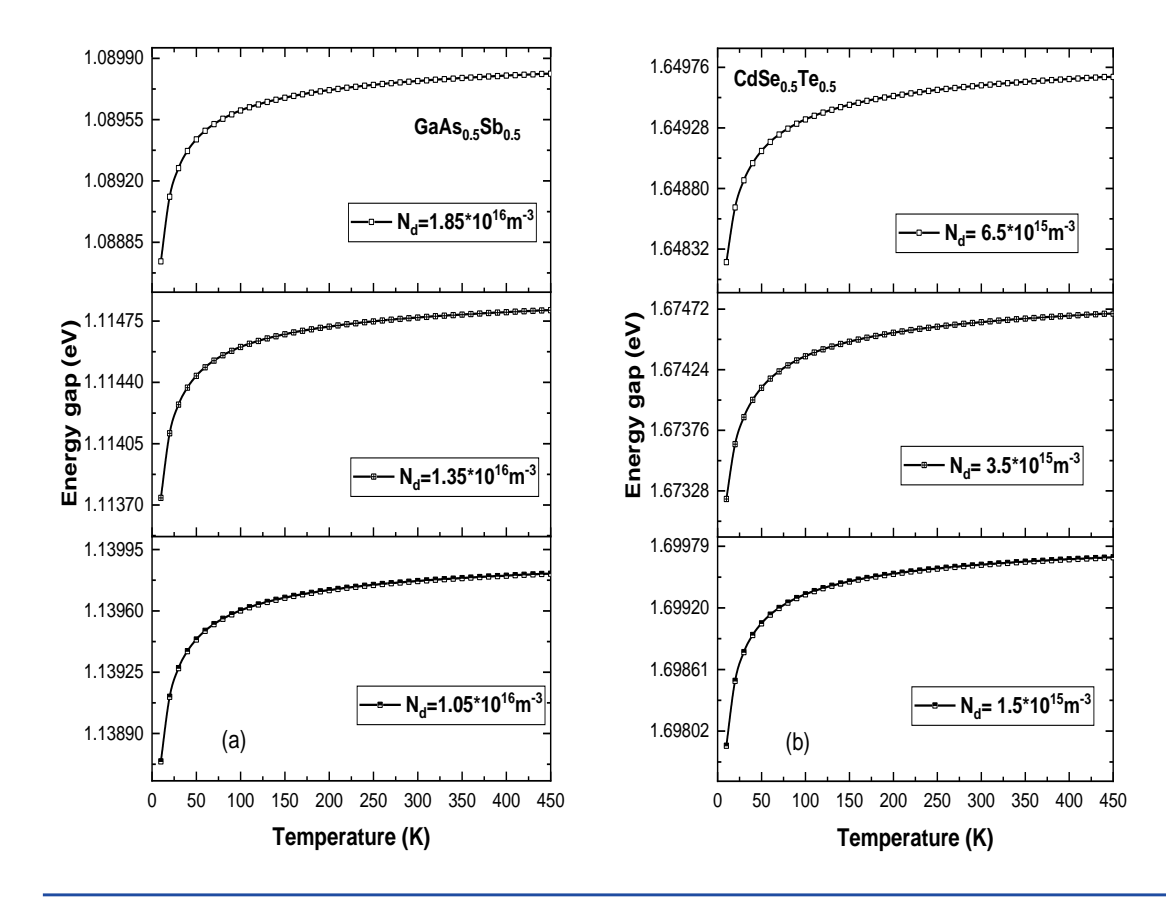


Figure 6. Energy gap of versus temperature according to doped non-degenerate Lanyon and Tuft approach of (a) $GaAs_{0.5}Sb_{0.5}$ alloy, (b) $CdSe_{0.5}Te_{0.5}$ alloy.

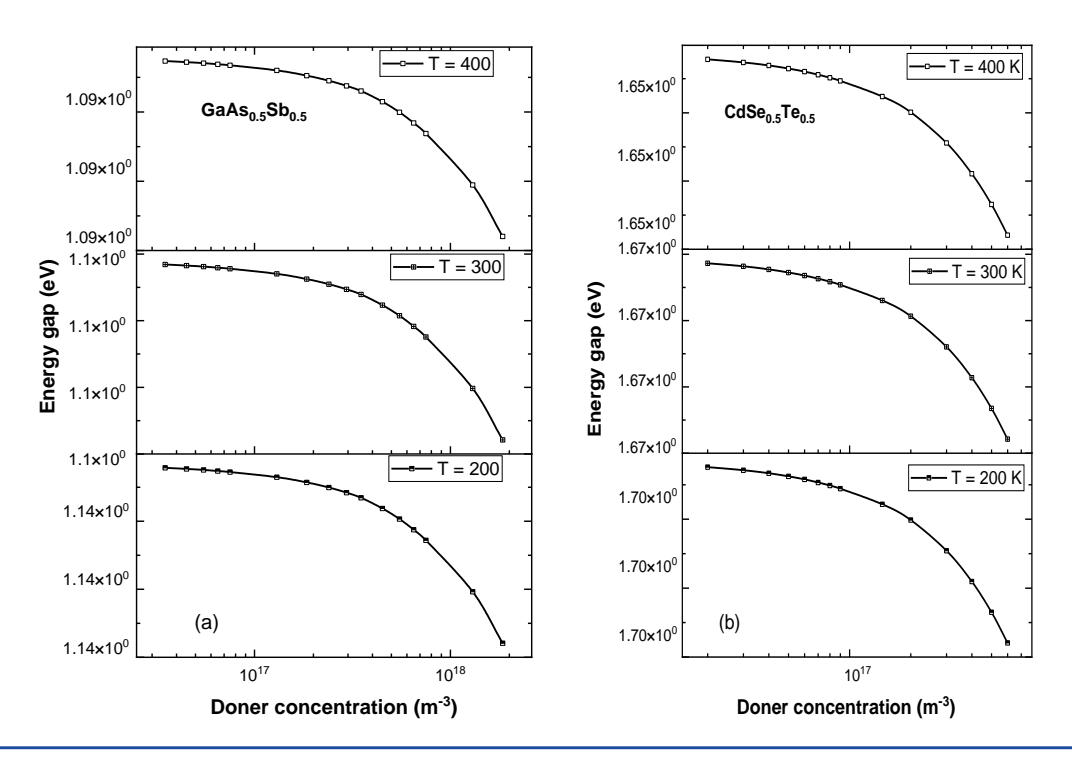


Figure 7. Energy gap according to Lanyon and Tuft approach versus doner concentration of doped non-degenerate (a) $GaAs_{0.5}Sb_{0.5}alloy$, (b) $CdSe_{0.5}Te_{0.5}$ alloy.

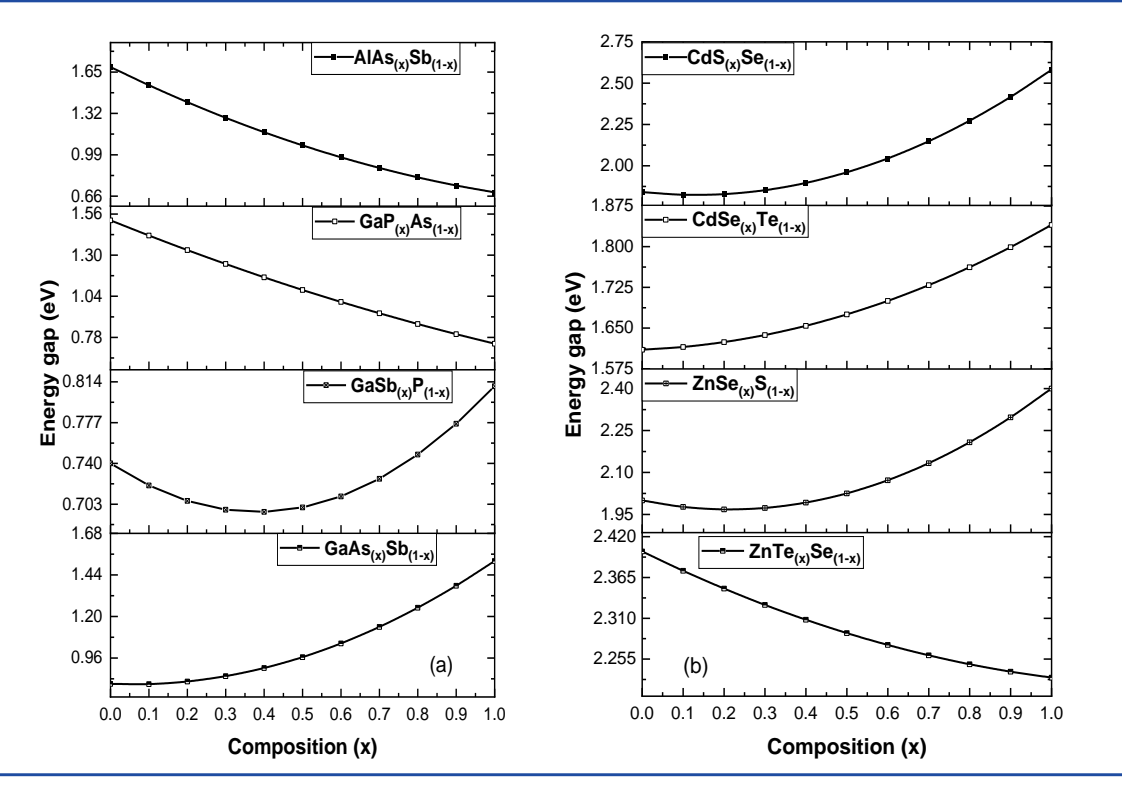


Figure 8. : Energy gap versus composition at 300K calculated according to doped degenerate Lanyon and Tuft approach of (a) III-V ternary semiconductor alloys, (b) II-VI ternary semiconductor alloys.

Figure 8b shows the energy gap of doped-degenerate II-VI ternary semiconductor alloys versus composition at 300K and $N_d = 3 \times 10^{18} \mathrm{m}^{-3}$ according to Lanyon and Tuft approach. The energy gap of $CdS_{(x)}Se_{(1-x)}$ increases continuously as the CdS composition increases. Similarly, in $CdSe_{(x)}Te_{(1-x)}$ it increases as the CdSe composition increases. The energy gap for $ZnSe_{(x)}S_{(1-x)}$ shows non-linear behaviour, initially dropping with increasing ZnSe composition up to about x = 0.2, then increasing. The energy gap of $ZnTe_{(x)}Se_{(1-x)}$ decreases as the ZnTe composition increases [35-36,41].

The effect of temperature on the energy gap of some selected ternary alloys from III-V and II-VI semiconductors in a temperature range up to 450 K is shown in **Figure 9**. The estimation follows the semi-empirical approach at doped degenerate conditions and essential bowing parameter model with the aid of the parameters listed in Table 2. **Figure 9a** demonstrates the energy gap of doped degenerate $GaAs_{0.5}Sb_{0.5}$ as a function of temperature at various donor concentrations $(7.25 \times 10^{18} \ m^{-3}, 1.15 \times 10^{19} \ m^{-3} \ and 1.27 \times 10^{20} \ m^{-3})$

while **Figure 9b** depicts such dependence for $CdSe_{0.5}Te_{0.5}$ at various donor concentrations $(7.25 \times 10^{18}~m^{-3}, 1.15 \times 10^{19}~m^{-3})$ and $1.27 \times 10^{20}~m^{-3}$). The energy gap of the two ternary alloys decreases monotonically with rising the temperature in the examined temperature range. At selected temperature, increasing the doping concentration appears to result in a little decrease in the energy gap [37-40].

Figures 10a and 10b illustrate the relationship between the energy gap and donor concentrations of one example of doped degenerate III-V ternary alloy ($GaAs_{0.5}Sb_{0.5}$) and one of doped degenerate II-VI ternary alloy ($CdSe_{0.5}Te_{0.5}$), respectively, at some temperatures (200 K, 300 K, and 400 K) calculated by bowing parameter model that and Lanyon and Tuft doped degenerate approach. The energy gap decreases slightly with increasing donor concentration. At greater donor concentrations, the change in energy gap becomes more significant. Higher temperatures usually result in slightly lower energy gap values for a given donor concentration [40-47].

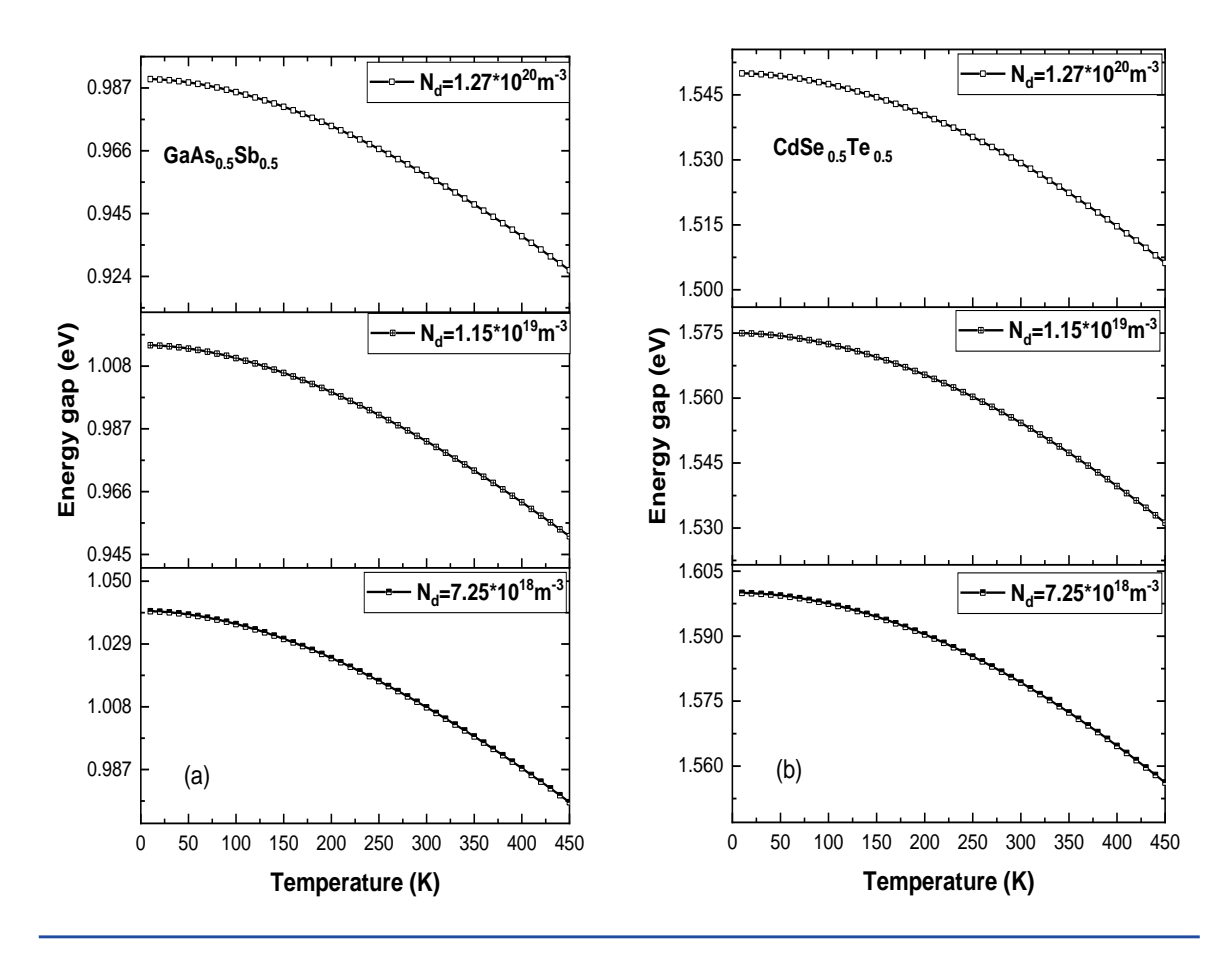


Figure 9. Energy gap versus Temperature of doped degenerate (a) $GaAs_{0.5}Sb_{0.5}$ alloy according to the Semi-Empirical approach, (b) $CdSe_{0.5}Te_{0.5}$ alloy according to the semi-empirical approach.

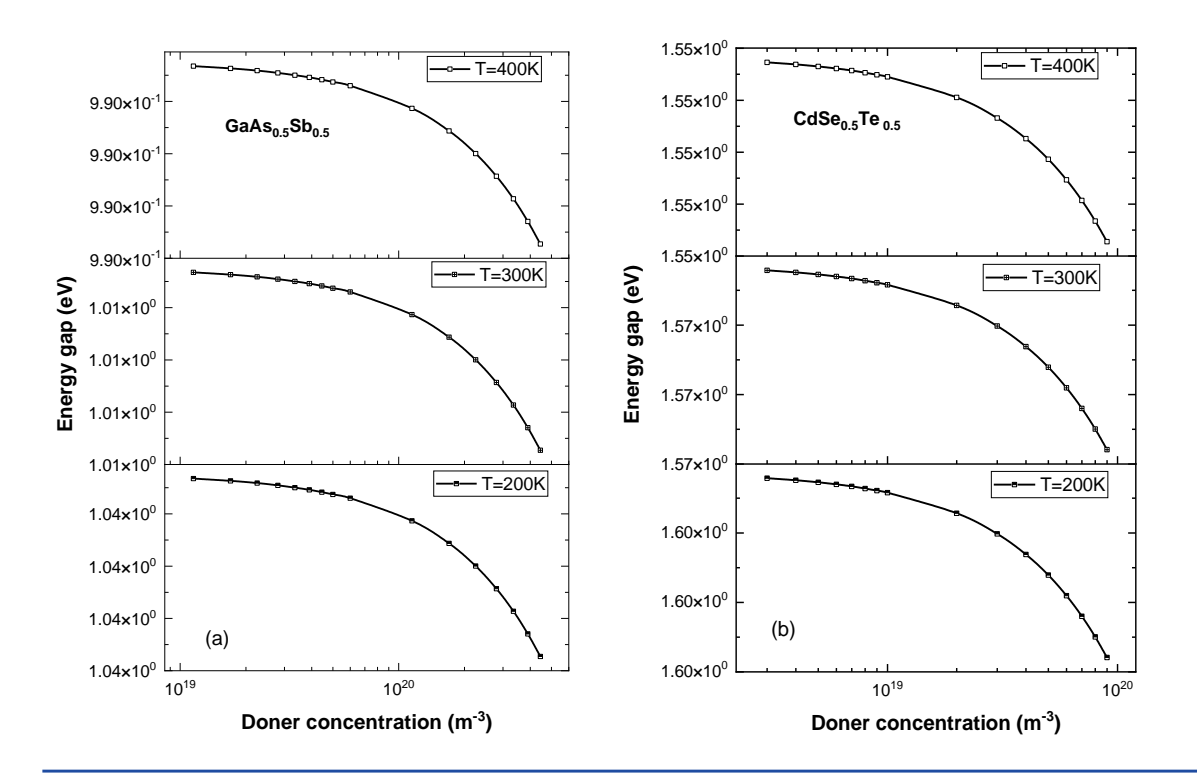


Figure 10. Energy gap versus doner concentration of doped degenerate: (a) $GaAs_{0.5}Sb_{0.5}$ alloy according to Lanyon and Tuft approach, (b) $CdSe_{0.5}Te_{0.5}$ alloy according to Lanyon and Tuft approach.

Table 1. Parameters of some semiconductor elements of group IV used in the calculation of energy gap of binary semiconductor alloys

Element	E_g (eV)	E g (0) (eV)	a (eVlK)	β (K)	$\gamma \ (J.m)$	arepsilon	m*/m 0
Si	1.12	1.17	4.73 x 10 ⁻⁴	636	1 x 10 ⁻²⁹	11.7	0.26
Ge	0.54	0.66	5.5 x 10 ⁻⁴	235	1 x 10 ⁻²⁹	16.2	0.55
C	5.47	5.47	1.5 x 10 ⁻⁴	2000	1 x 10 ⁻²⁹	5.5	1.1

Table 2. Parameters of some III-V and II-VI compound semiconductors used in the calculation of energy gap of ternary semiconductor alloys.

Compound	E_{g}	$E_{g}\left(0\right)$	а	β	γ	ε		$m^*/m_{\scriptscriptstyle o}$
	(eV)	(eV)	(eVlK)	(<i>K</i>)	(J.m)		r_s	
GaAs	1.723	1.52	4.1 x 10 ⁻⁴	204	1.1x10 ⁻²⁹	12.85	3.27	0.067
GaSb	0.907	0.81	4.4 x 10 ⁻⁴	200	1.4×10^{-27}	15.69	4.21	0.04
GaP	0.83	0.74	4.88 x 10 ⁻⁴	210	1×10^{-29}	11.11	4.36	0.07
AlAs	0.683	0.69	4.4 x 10 ⁻⁴	300	1×10^{-29}	10.06	4.7	0.15
AlSb	1.65	1.69	5.3 x 10 ⁻⁴	350	1×10^{-29}	12.04	3.32	0.41
ZnTe	2.56	2.23	4.9 x 10 ⁻⁴	400	1×10^{-29}	9.67	3.25	0.35
ZnSe	2.76	2.4	6 x 10 ⁻⁴	500	1×10^{-29}	9.2	3.16	0.49
ZnS	2.24	2	4.5 x 10 ⁻⁴	500	1×10^{-29}	8.32	3.43	0.29
CdSe	1.95	1.84	5.7 x 10 ⁻⁴	450	1×10^{-29}	9.6	3.62	0.13
CdTe	1.82	1.61	4.9 x 10 ⁻⁴	600	1×10^{-29}	10.76	3.71	0.08
CdS	2.76	2.58	4.7 x 10 ⁻⁴	800	1 x 10 ⁻²⁹	5.3	3.16	0.2

4. Conclusions

The energy band gap of some nominated binary and ternary semiconductor alloys have been investigated. This study reveals that the energy band gap of various undoped, doped non-degenerate, and doped degenerate semiconductor alloys is significantly influenced by alloy composition, doping concentration, and temperature. The observed variations in the band gap behaviour, ranging from linear to nonlinear, emphasize the necessity of integrating thermal and compositional engineering with doping strategies. These insights enhance the understanding of semiconductor properties and provide a framework for the predictive design of materials tailored for high-frequency electronic, photovoltaic, and optoelectronic applications.

References

- [1] Ludbrook, B. M.; Levy, G.; Nigge, P.; Zonno, M.; Schneider, M.; Dvorak, D. J.; Veenstra, C. N.; Zhdanovich, S.; Wong, D. W.; Dosanjh, P.; Straßer, C.; Stöhr, A.; Forti, S.; Ast, C. R.; Starke, U.; Damascelli, A. Evidence for superconductivity in Lidecorated monolayer graphene. Proc. Natl. Acad. Sci. U.S.A. 2015, 112 (38), 11795–11799.
- [2] Ghosh, S. K.; Mandal, D. High-performance biopiezoelectric nanogenerator made with fish scale. Appl. Phys. Lett. 2016, 109 (10), 103701.
- [3] Mourad, D.; Czycholl, G.; Kruse, C.; Klembt, S.; Retzlaff, R.; Hommel, D.; Gartner, M.; Anastasescu, M. Band gap bowing of binary alloys: Experimental results compared to theoretical tight-binding supercell calculations for Cd_x Zn_(1-x) Se. Phys. Rev. B 2010, 82, 165204.
- [4] Bansal, B.; Ghosh, R.; Venkataraman, V. Scattering of carriers by charged dislocations in semiconductors. J. Appl. Phys. 2013, 113, 163705.
- [5] Shi, X.; Wei, Y.; Yan, R.; Hu, L.; Zhi, J.; Tang, B.; Li, Y.; Yao, Z.; Shi, C.; Yu, H.; Huang, W. Leaf Surface-Microstructure Inspired Fabrication of Fish Gelatin-Based Triboelectric Nanogenerator. Nano Energy. 2023, 104, 107964.
- [6] Senn, M. S.; Bombardi, A.; Murray, C. A.; Vecchini, C.; Scherillo, A.; Luo, X.; Cheong, S. W. Negative thermal expansion in hybrid improper ferroelectric Ruddlesden-Popper perovskites by symmetry trapping. Phys. Rev. Lett. 2015, 114, 035701.
- [7] Strzałkowski, K.; Abouais, A.; Alaoui-Belghiti, A.; Singh, D.; Hajjaji, A. Alloy Disordering Effects on the Thermal Conductivity and Energy Gap Temperature Dependence of Cd_(1-x) Z_x Se Ternary Crystals Grown by the Bridgman Method. Materials 2023, 16, 3945.
- [8] Tarbi, A.; Chtouki, T.; Elkouari, Y.; Erguig, H.; Migalska-Zalas, A.; Aissat, A. Bandgap Energy Modeling of the Deformed Ternary GaAs1-uNu by Artificial Neural networks. Heliyon. 2022, 8, e10212.
- [9] Kim, J.; Nasrun, R. F. B.; Jeong, W. H.; Shen, X.; Sausan, I. S.; Kim, D.; Seok, G. E.; Jung, E. D.; Kim, J. H.; Lee, B. R. Conjugated Polyelectrolytes as a

- Defect-Passivating Hole Injection Layer for Efficient and Stable Perovskite Light-Emitting Diodes. ACS Appl. Electron. Mater. 2024, 6 (12), 8929–8937.
- [10] Cho, S.; Lim, J.; Seo, Y. (2023). Fabrication of Bismuth–Antimony–Telluride Alloy/Poly (3, 4ethylenedioxythiophene) Hybrid Films for Thermoelectric Applications at Room Temperature by a Simple Electrochemical Process. Chem. Mater. 2023, 35, 3196-3205.
- [11] Charifi, Z.; Hassan, F. E. H.; Baaziz, H.; Khosravizadeh, S.; Hashemifar, S. J.; Akbarzadeh, H. Structural and electronic properties of the wide-gap Zn1- xMgxS, Zn1- xMgxSe and Zn1-xMgxTe ternary alloys. J. Phy.: Condensed Matter. 2005, 17, 7077.
- [12] Khomyakov, P. A.; Luisier, M.; Schenk, A. Compositional bowing of band energies and their deformation potentials in strained In_x Ga_(1-x) As ternary alloys: a first-principles study. Appl. Phys. Lett. 2015, 107, 062104.
- [13] Shen, J.-X.; Wickramaratne, D.; Van de Walle, C. G. Band bowing and the direct-to-indirect crossover in random BAIN alloys. Phys. Rev. Mater. 2017, 1, 065001.
- [14] Bonsignore, G.; Agliolo Gallitto, A.; Agnello, S.; Barbera, M.; Candia, R.; Cannas, M.; Collura, A.; Dentici, I.; Gelardi, F. M.; Lo Cicero, U.; Montagnino, F. M.; Paredes, F.; Sciortino, L. Electrical-optical characterization of multijunction solar cells under 2000X concentration. AIP Conf. Proc. 2014, 1616, 102.
- [15] Chen, D.; Ravindra, N. M. Structural, Thermodynamic, and Electronic Properties of GaP_x Sb_(1-x) and InP_x Sb_(1-x) Alloys. Emerg. Mater. Res. 2013, 2, 109–113.
- [16] Zaitsev, I.; Corley-Wiciak, A. A.; Corley-Wiciak, C.; Zoellner, M. H.; Richter, C.; Zatterin, E.; Manganelli, C. L. (2024). The Interplay between Strain, Sn Content, and Temperature on Spatially Dependent Bandgap in Ge1- x Snx Microdisks. Phys. Status Solidi (RRL)–Rapid Research Letters. 2024, 18, 2300348.
- [17] Wendav, T.; Fischer, I. A.; Montanari, M.; Zoellner, M. H.; Klesse, W.; Capellini, G.; Schulze, J. Compositional dependence of the band gap of Ge_(1-x) Si x alloys. Appl. Phys. Lett. 2016, 108, 242104.
- [18] Polimeni, A.; Capizzi, M.; Nabetani, Y.; Ito Y; Okuno T.; Kato T.; Matsumoto T.; Hirai T. Temperature dependence and bowing of the bandgap in ZnSe1- x Ox. Appl. Phys. lett. 2004, 84, 3304-6.
- [19] Abdullah, T.; Sami, S. A.; Omar, M. S. Temperature Dependence of the Energy Band Gap of CuSi_2 P_3 Semiconductor Using PSOPW Method. Mater. Sci. Poland 2018, 36, 553–560.
- [20] Nepal, N.; Li, J.; Nakarmi, M. L.; Lin, J. Y.; Jiang, H. X. Temperature and Compositional Dependence of the Energy Band Gap of Al_x Ga_(1-x) N Alloys. Appl. Phys. Lett. 2005, 87, 242104.

- [21] Katz, O.; Meyler, B.; Tisch, U.; Salzman, J. Determination of Bandgap Bowing for Al_x Ga_(1-x) N Alloys. Phys Status Solidi. 2001, 188, 789-792.
- [22] Lanyon, H. P. D.; Tuft, R. A. Bandgap narrowing in moderately to heavily doped silicon. IEEE Trans. Electron Devices 1979, 26, 1014–1018.
- [23] Lu, J. G.; Fujita, S.; Kawaharamura, T.; Nishinaka, H.; Kamada, Y.; Ohshima, T.; Zhao, B. H. Carrier concentration dependence of band gap shift in n-type ZnO:Al films. J. Appl. Phys. 2007, 101, 083701.
- [24] Mazhukin, V. I.; Koroleva, O. N.; Mazhukin, A. V.; Aleshchenko, Y. A. Effect of degenerate carriers on Si band gap narrowing. Bull. Lebedev Phys. Inst. 2017, 44, 198–201.
- [25] Varshni, Y. P. Temperature dependence of the energy gap in semiconductors. Physica 1967, 34, 149–154
- [26] Chen, Z.; Diebels, S.; Peter, N. J.; Schneider, A. S. Identification of finite viscoelasticity and adhesion effects in nanoindentation of a soft polymer by inverse method. Comp. Mater. Sci. 2013, 72, 127-139.
- [27] Bahadur, A.; Mishra, M. Dependence of Ionicity and Mechanical Properties on Valence Electron Density in Binary Tetrahedral Semiconductors. J. Res. Phys. 2012, 36, 31.
- [28] Yadav, D. S.; Verma, A. S. Electronic, Optical and Mechanical Properties of AII–BVI Semiconductors. Int. J. Mod. Phys. B. 2012, 26, 1250020.
- [29] Foti, A.; Calì, L.; Petralia, S.; Satriano, C. Green Nanoformulations of Polyvinylpyrrolidone-Capped Metal Nanoparticles: A Study at the Hybrid Interface with Biomimetic Cell Membranes and In Vitro Cell Models. Nanomaterials, 2023, 13, 1624.
- [30] Regiel-Futyra, A.; Kus-Liskiewicz, M.; Sebastian, V.; Irusta, S.; Arruebo, M.; Stochel, G.; Kyzioł, A. Development of Noncytotoxic Chitosan–Gold Nanocomposites as Efficient Antibacterial Materials. ACS Appl. Mater. Interfaces 2015, 7, 1087–1096.
- [31] Ramezanpour, A.; Ansari, L.; Rahimkhoei, V.; Sharifi, S.; Bigham, A.; Lighvan, Z. M.; Rezaie, J.; Szafert, S.; Mahdavinia, G. R.; Akbari, A.; Jabbari, E. Recent Advances in Carbohydrate-Based Paclitaxel Delivery Systems. Polym. Bull. 2024, 81, 1043–1069.
- [32] Mohammadi, S.; Kaur, N.; Radu, D. R. Nanoscale Cu_2 ZnSnS_x Se_(4-x) (CZTS/Se) for Sustainable Solutions in Renewable Energy, Sensing, and Nanomedicine. Crystals. 2024, 14, 479.
- [33] Maskar, E.; Lamrani, A. F.; Belaiche, M.; Es-Smairi, A.; Rai, D. P.; Fazouan, N. (2021). First principles study of electronic, optical and transport properties of bulk and monolayer SnO. Superlattices Microstruct. 2021, 150, 106776.
- [34] Arimondo, E.; Ciampini, D.; Rizzo, C. Spectroscopy of Natural and Artificial Atoms in Magnetic Fields. In: Advances in Atomic, Molecular, and Optical Physics; Elsevier, 2016. Vol. 65, p. 1–66.
- [35] Xiang, D.; Wang, D.; Zheng, T.; Chen, Y. Effects of Rare Earths on Microstructure and Wear Resistance in Metal Additive Manufacturing: A Review. Coatings. 2024, 14, 139.

- [36] Wang, L.; Wang, X.; Liu, T.; Sun, F.; Li, S.; Geng, Y.; Fu, J. (2023). Bio-inspired self-healing and anti-corrosion waterborne polyurethane coatings based on highly oriented graphene oxide. npj Mater. Degrad. 2023, 7, 96.
- [37] Lou, J.; Ren, K.; Huang, Z.; Huo, W.; Zhu, Z.; Yu, J. Electronic and optical properties of two-dimensional heterostructures based on Janus XSSe (X= Mo, W) and Mg(OH)₂: A first principles investigation. RSC advances. 2021, 11, 29576-29584.
- [38] Nasir, S.; Chee, F. P.; Ghosh, B. K.; Rumaling, M. I.; Rasmidi, R.; Duinong, M.; Juhim, F. Composition Dependence Structural and Optical Properties of Silicon Germanium (Si_x Ge_(1-x)) Thin Films. Crystals. 2023, 13, 791.
- [39] Sarangapani, P.; Chu, Y.; Charles, J.; Klimeck, G.; Kubis, T. Band-Tail Formation and Band-Gap Narrowing Driven by Polar Optical Phonons and Charged Impurities in Atomically Resolved III–V Semiconductors and Nanodevices. Phys. Rev. Appl. 2019, 12, 044045.
- [40] Smith, K. T.; Gorsak, C. A.; Buontempo, J. T.; Cromer, B. J.; Ikenoue, T.; Gulupalli, H.; Thompson, M. O.; Jena, D.; Nair, H. P.; Xing, H. G. Chasing Schottky–Mott: Metal-First Non Alloyed Contacts to β-Ga_2 O_3 for Interface Quality and Minimal Surface Modification. J. Appl. Phys. 2024, 136, 215302.
- [41] Kim, B. W.; Park, S. H.; Kapadia, R. S.; Bandaru, P. R. Evidence of Percolation-Related Power Law Behavior in the Thermal Conductivity of Nanotube/Polymer Composites. Appl. Phys. Lett. 2013, 102, 243105.
- [42] Ning, J.; Lei, W.; Yang, J.; Xi, J. First-principles Study of the Temperature-Induced Band Renormalization in Thermoelectric Filled Skutterudites. Phys. Chem. Chem. Phys. 2023, 25, 26006–26013.
- [43] Bisti, V. E.; Kirova, N. N. Cyclotron Excitations in Pure Bilayer Graphene: Electron–Hole Asymmetry and Coulomb Interaction. Physica B: Condensed Matter. 2012, 407, 1923-1926.
- [44] Dahlinger, M.; Carstens, K. Band Gap Narrowing Models Tested on Low Recombination Phosphorus Laser Doped Silicon. J. Appl. Phys. 2016, 120, 155701.
- [45] Pramanik, M. B.; Al Rakib, M. A.; Siddik, M. A.; Bhuiyan, S. Doping Effects and Relationship between Energy Band Gaps, Impact of Ionization Coefficient and Light Absorption Coefficient in Semiconductors. Eur. J. Eng. Technol. Res. 2024, 9, 10–15.
- [46] Russell, H. B.; Andriotis, A. N.; Menon, M.; Jasinski, J. B.; Martinez-Garcia, A.; Sunkara, M. K. Direct Band Gap Gallium Antimony Phosphide (GaSb_x P_(1-x)) Alloys. Sci. Rep. 2016, 6, 20822.
- [47] Remeš, Z.; Stuchlík, J.; Kupčík, J.; Babčenko, O. Thin Hydrogenated Amorphous Silicon Carbide Layers with Embedded Ge Nanocrystals. Nanomaterials. 2025, 15, 176.